This is a peer-reviewed, accepted author manuscript of the following article:
Chen, Y., Li, T., Zeng, P., Ma, J., Patelli, E., & Edwards, B. (2020).
Dynamic and probabilistic multi-class prediction of tunnel squeezing intensity.
Rock Mechanics and Rock Engineering. https://doi.org/10.1007/s00603-020-02138-8

Abstract

Tunnel squeezing is a time dependent process that typically occurs in weak or over-stressed rock masses, significantly influencing the budget and time of tunnel construction. This paper presents a new framework to probabilistically predict the potential squeezing intensity, and to dynamically update the prediction during construction based on the sequentially revealed ground information. An extensively well documented database, which contains quantitative data from 154 squeezing sections with 95 unpublished inventories is established. A Decision Tree method is employed to train a probabilistic multi-classification model to predict the tunnel squeezing intensity. The trained classifier is then integrated with a Markovian geologic model, which features embedded Bayesian updating procedures, to achieve a dynamic prediction on the state probabilities of the geologic parameter within the Markovian geologic model and the resulting squeezing intensity during excavation. An under-construction tunnel case —Miyaluo #3 tunnel— is used to illustrate the proposed framework. Results show that the Decision Tree classifier, as opposed to other black-box models, is easily to be interpreted. It provides reliable predictive accuracy while leading to insights into the understanding of squeezing problem. The strength-stress ratio (*SSR*) is suggested to be the most important factor. Moreover, the implementation of the updating procedures is efficient since only simple field test (eg. Point Load index or Schmidt rebound index) is required. Multiple rounds of predictions within the updating process allow different levels of prediction, for example long-range, short-term, or immediate, to be extracted as useful information towards the decision-making of construction operations. Therefore, this framework can serve as a pragmatic tool to assist the selection of optimal primary-support and other construction strategies based on the potential squeezing risk.

Keywords: Tunnel squeezing; Multi-classification; Dynamic prediction; Decision tree; Bayesian updating; Markov process

List of Symbols

N_c (or α) competency factor;

SSR strength stress ratio;

σ_{ci} uniaxial compressive strength of intact rock;

σ_{cm} rock mass uniaxial compressive strength;

γ rock mass weight;

H burial depth of tunnel;

Q rock quality index;

RMR rock mass rating;

N rock mass number;

SRF stress reduction factor;

B or *D* tunnel diameter;

K support stiffness.

GC Surrounding rock classes based on BQ system

σ_θ tangential stress;

ε percentage strain (ratio of tunnel closure *u* to tunnel diameter *D*);

p_0 in situ vertical stress at tunnel depth;

p_i rock support pressure;

θ_i the threshold used to split a node in the Decision Tree

A Transition intensity matrix

V Interval transition matrix

L Likelihood matrix

t_i a location variable in the Markov geologic model

X_R the geologic parameter that follows a discrete state, continuous space Markov process

$\mathbf{s}(t_i)$ a vector representing the state probabilities of the geologic parameter X_R at location t_i

m a vector representing the mean values of each parametric state range of X_R

$E(X_R)$ the integrated strength variable showing the weighted average of intact rock strength based on the scalar product of vector **s** and **m**

$\overline{\sigma}_{cm}$ a variable representing the integrated value of the rock mass strength at a certain tunnel face

PLI Point Load index

SHR Schmidt Hammer rebound index

1 Introduction

Tunnel squeezing is a time-dependent process associated with the plastic flow (creep) of rock masses, typically occurring in high geostress backgrounds when tunneling through weak rock masses, such as phyllite, mudstone, fault fracture zones and other problematic geological combinations (Aydan et al. 1993; Barla 1995; Hoek and Marinos 2000). Prediction of tunnel squeezing remains a key problem to ensure the safety of tunneling process, as excessive deformation resulted from squeezing may lead to severe support damage and significant economic consequences, plus construction time overruns (Hoek 2001; Singh et al. 2007; Jimenez and Recio 2011; Feng and Jimenez 2015).

Many empirical formulations towards this goal, based on history cases, have been developed due to simplicity and ease of use. Focused on different perspectives and factors, three types of formulae can be summarized from literature (see Table 1): (i) Geomechanical-based methods: a demarcation line is drawn to classify squeezing and non-squeezing cases, according to the combinations of tunnel depth and rock mass quality (Singh et al. 1992; Goel et al. 1995; Dwivedi et al. 2013). *RMR* and *Q* values are commonly involved since they are routinely recorded in rock tunneling history, so that empirical relations concerning the occurrence of squeezing can be developed (Jimenez and Recio 2011). (ii) Competence-factor based methods: there are many empirical expressions focusing on the concept of competence factor, which is also known as *SSR* (i.e. the ratio between rock mass strength and stress), as it intrinsically formulates the state of weak rock masses in an overstressed setting (Jethwa 1981; Barla 1995; Aydan et al. 1996; Hoek 2001). (iii) Probabilistic methods: given the significant uncertainties involved in the tunneling process (Panthi and Nilsen 2007; Sousa and Einstein 2012), some researchers have recently evaluated the likelihood of tunnel squeezing in a probabilistic way, for its unique merit to be naturally extended to risk assessment (Panthi and Nilsen 2007; Jimenez and Recio 2011; Feng and Jimenez 2015; Sun et al. 2018).

However, despite the prospect of probabilistic analyses, binary predictive methods have relatively limited use in tunneling practice because they can only output dichotomous outcomes: squeezing or non-squeezing. By contrast, a probabilistic prediction with respect to the extent of tunnel squeezing, or as referred to as multi-class probabilistic classification, is of greater interests since it can further lead to an optimal selection of primary-support strategy based on the risk of potential squeezing severity (Hoek 2001; Panthi and Nilsen 2007).

In addition, another challenge in terms of a reliable prediction is that the geologic conditions of surrounding rocks obtained in the investigation stage are often incomplete and unreliable (Ioannou 1987; Einstein 2007; Guan et al. 2012). Therefore, such inconsistencies between investigation and construction significantly reduces the accuracy of those aforementioned methods. As such, a dynamic scheme based on excavated grounds to predict the squeezing hazard, especially in a multi-class and probabilistic manner, is very useful because it can

reasonably boost the reliability and practicality of the prediction of squeezing.

To that end, this paper presents a novel framework that achieves the multi-class probabilistic classification of squeezing intensity in a dynamic way. In particular, this framework consists of two main components: (i) a probabilistic classifier that outputs multi-class probability distributions of squeezing intensity and (ii) a Markovian geologic model that stochastically models the ground conditions. These two components are combined through a Bayesian updating process of an important predictor: strength stress ratio (*SSR*). For this system to work, an enriched database containing 154 tunnel squeezing inventories is employed to train the multi-class classifier using the Decision Tree algorithm. Once trained, a prior prediction on squeezing intensity for the whole tunnel alignment can be made, based merely on the preliminary investigation information. During tunneling process, via the field characterization provided by certain exploration program on each newly excavated tunnel face, posterior predictions on squeezing intensity at any location along the tunnel can be sequentially updated. With the tunnel face advances round by round, the updating process continues dynamically. Finally, such framework is illustrated through a real under-construction tunnel case to demonstrate its applicability in engineering practice.

[Table 1 approximately here]

2 Methodology for multi-class probabilistic prediction

2.1 Predictors and Data for training

2.1.1 Predictors

As previous classical empirical models suggested (Table 1), three parameters, namely *H*, *Q* and *SSR* are historically the most popular indicators. Still, despite the universality of such features, there exists variations and modifications due to the accessibility of reliable data in field: such as the replacement of *Q* value with a rock mass number *N* due to the uncertainties in obtaining *SRF* in the field (Goel et al. 1995; Dwivedi et al. 2013), and the common use of vertical stress when deriving *SSR*, neglecting the influence of tectonic stress (Jethwa 1981; Barla 1995; Aydan et al. 1996; Hoek 2001; Feng and Jimenez 2014).

Besides these efforts, some complementary factors that affect the squeezing behavior in other ways have also been proposed in recent years. The support stiffness (*K*) is considered of playing an important role in the deformation of tunnel due to the interaction of support pressure and the deforming response of the rock masses (Dwivedi et al. 2013; Feng and Jimenez 2015), as the undesirable deformation may be arrested if adequate support system is provided in appropriate timing (Jethwa 1981). In addition, according to Goel (1995), squeezing behavior is also affected by the size of opening. This means the scale effects of the tunnel excavation, represented by the tunnel diameter (*D*), should also be taken into consideration (Dwivedi et al. 2013; Feng and Jimenez 2015; Sun et al. 2018).

Despite the intention to construct a predictive model with more factors of squeezing behavior, but given the limit of data availability, which is a major concern for training-based supervised learning methods, we finally employed five significant factors in this analysis to conduct a training process for a multi-class probabilistic classifier. Table 2 lists these predictors as well as the approaches used to derive them. In particular, a *GC* variable based on the BQ system, the Chinese standard for engineering classification of rock masses, is used because 108 out of 154 tunnel squeezing cases in the database (Appendix A) are sourced from tunnel projects in China, in which the *GC* class, as opposed to the *Q* value, are routinely documented on field. An overview of the BQ system is provided in Appendix B.

[Table 2 approximately here]

2.1.2 Description of the tunnel squeezing database

The database of case histories employed in this work is reproduced in Appendix A. This unprecedentedly comprehensive database contains complete information concerning five predictors (Table 2)—Buried Depth (*H*), Strength-Stress Ratio (*SSR*), Support Stiffness (*K*), Rock Mass Class (*GC*), Diameter (*D*)—of 154 tunnel

squeezing sections from 31 tunnel projects around the world, which to our knowledge is the most detailed databases with respect to squeezing inventories as of now. Among which, 59 cases are referenced from literature (Kimura et al. 1987; Steiner 1996; Chern et al. 1998; Hoek 2001; Dalgıç 2002; Jing-Yu et al. 2002; Liu et al. 2005; Sanhui and Runqiu 2005; Panthi 2006; Shrestha 2006; Ye-yan 2007; Panthi and Nilsen 2007; Singh et al. 2007; Shuishan 2009; Fujun 2010; SUN 2010; Jimenez and Recio 2011; Basnet 2013; Dwivedi et al. 2013; Feng and Jimenez 2015); and more importantly, many others (95 cases) are unpublished cases from pivotal highway/railway projects constructed in southwest China, in which the authors' research group had been closely involved over years. Although several databases had been established before, as shown in the last column of Table 1, the challenge is that old databases are short of information about some new features, such as Support Stiff (K) or Tunnel Diameter (D) (Goel et al. 1995; Goel and Swarup 2006; Jimenez and Recio 2011; Shafiei et al. 2012), while some recent databases are indeed incomplete (Feng and Jimenez 2015).

[Figure 1 approximately here]

[Table 3 approximately here]

[Figure 2 approximately here]

Fig. 1 displays an overview of the tunnel squeezing cases in the database. For each case, besides the data of five predictors, it also contains a quantitative percentage strain (ε) that indicates the severity of the squeezing condition. Despite the universality of the strain index, which is defined as the ratio of tunnel closure to tunnel diameter, the relationship between the strain and squeezing intensity has not reached an agreement among researchers (see Table 3) (Aydan et al. 1996; Sakurai 1997; Singh and Goel 1999; Hoek and Marinos 2000). As a result, of the 154 cases in the database, the distributions of squeezing intensity are shown in Fig. 2 according to three popular multi-class schemes plus one binary scheme of squeezing intensity classification in Table 3. Unlike the inconsistency of the thresholds regarding the multi-class situation, the tunneling community has shared one widely-recognized binary threshold in differentiating squeezing and non-squeezing situations: ε = 1% (Sakurai 1997; Hoek 2001; Jimenez and Recio 2011; Feng and Jimenez 2015; Sun et al. 2018). It should be specifically noted that such thresholds of strain levels are indeed indicators, instead of guarantees, of likely stability problems (Hoek 2001). In more detail, Fig. 3 shows the histograms as well as additional summary statistics: average, median, skewness and kurtosis of the five predictors considered to train the classifier.

[Figure 3 approximately here]

2.2 Training models and validation

The Decision Tree method, with explicit conjunctions of predictors, is easy to be interpreted and analyzed in terms of the classification results and the classifying process, compared to other black-box classifiers (e.g., neural network and support vector machine). Therefore, the main advantage is the capability to provide useful insights for the understanding of the squeezing problem in the analysis.

2.2.1 Definition and structure

As a common supervised learning method with many modern applications (Breiman 2001; Hastie et al. 2009), Decision Tree is a binary tree-like structure classifier, which is constructed (or learned) by repeatedly splitting a node into two child nodes. It starts with the root node that contains the whole training dataset—a set of historical data with pre-assigned classes for all observations. Each child node equivalents to a subset containing part of training samples, and the leaf nodes represent the class labels. Conceptually, the constructing process of a classification tree works top-down, following the decisions from the root node all the way down to the leaf nodes. At each node, as explained in Fig. 4a, the parent node is split only by one predictor through a certain binary criterion at a time, for example the inequation with threshold θ_i compared to each value (shown as x_i) of the predictor X_i for all the samples in the parent node. Such inequality would further lead to two separate child nodes (subsets).

As illustrated in Fig. 4b and Fig. 4c, during the successive splitting process of the nodes (Fig. 4c), the tree method is essentially creating rectangular subsets of learning data (Fig. 4b) through one specific predictor at each node (i.e. the splitting of each node equivalents to the partitioning of training data). The branches represent conjunctions of features that lead to class labels. This partitioning process is repeated in a recursive manner and stops once the leaf nodes merely contain observations of one class label, as referred as “pure classification”, or when the relative decrease in impurity satisfies a certain threshold. The optimal selection of the predictor as well as the best split criterion at each node is made among innumerable possibilities and guided by impurity metrics in order to perfectly classify the samples to each class. Different impurity metrics are used by variants of the Decision Tree algorithms: such as the Gini impurity used by the CART algorithm, information gain used by C4.5 and C5.0 algorithm (Breiman 2001; Wu et al.2008; Loh 2014).

[Figure 4 approximately here]

2.2.2 Node purity function

C5.0 algorithm, as the latest successor of the C4.5 algorithm, has several new capabilities and much-improved efficiency over C4.5 (Wu et al. 2008). Hence C5.0 algorithm is adopted in this analysis to choose the best split in the tree growing process. At each node, of all possible ways of splitting considered, the one which leads to

the greatest information gain is desired. The information gain is defined as the difference of entropy between before and after the split of the at any interior node. Take the nodes in Fig. 4a as an example:

$$gain(split = X) = info(n) - info_X(n) \tag{1}$$

where *info*(*n*) represents the entropy of node n_{Parent} prior to split and $info_X(n)$ is the expected entropy after the split by variable X_i. These two entropies are calculated respectively as follows (Kuhn and Johnson 2013):

$$info(n) = -\sum_{i=1}^{k} p_i \cdot log_2 p_i \tag{2}$$

$$info_X(n) = \frac{|n_{Left}|}{|n|} \cdot info(n_{Left}) + \frac{|n_{Right}|}{|n|} \cdot info(n_{Right}) \tag{3}$$

where k and p_i represent the number of classes and the percentage of each class in the n_{Parent} node respectively; n_{Left} and n_{Right} correspond to the two subsets of node n_{Parent}.

2.2.3 Pruning the tree structure

Normally, the attempt to perfectly classify the training samples would cause the tree structure to go excessively complex, thus overfitting the training data. The C5.0 algorithm adopts a post-pruning strategy that first allows the tree to grow fully and then prune nodes and branches having little effect on classification accuracy (Lantz 2013). The cross-validated accuracy is therefore employed to pursue the balance between efficiency and accuracy.

2.3 The best multi-class probabilistic classifier

Given the variance of classification schemes with respect to squeezing intensity (see Table 3 and Fig. 2), we build three multi-class trees plus one binary tree as a reference, according to the four schemes in Fig. 2, with each tree trained by all five predictors in Table 2. To evaluate the performance of the trained models, 10-fold cross-validation is employed to keep against over-fitting and obtain unbiased out-of-sample accuracy of the results. It is also used to prune the tree structure as mentioned in Section 2.2.3.

[Figure 5 approximately here]

As a result, Fig. 5 shows the performance of all the trained models. It turns out that the Singh-tree model has the best performance among multi-class classifiers, approximating a three-quarter predictive accuracy (75.19%). In contrast, the other two multi-class alternatives are noticeably inferior to the Singh-tree model, with a 10~15% predictive power loss. This decrease might be partially attributed to the fact that the Singh's scheme of squeezing intensity classification has four categories whereas Aydan and Hoek both have five categories, as shown in Table 3. In general principle, more categories result in less samples in each category, making it harder to output a reliable classification.

[Figure 6 approximately here]

Fig. 6 thusly displays the confusion matrix of the best-trained multi-class classifier (namely the Singh tree model) as well as the Binary tree model. Ideally, the confusion matrix would be diagonally dominant, indicating most predictions have been correctly labelled. Through color-labeling, it's evident to notice that Singh tree model is significantly less accurate when predicting "moderate squeezing" cases, compared to other three squeezing-intensity situations (Fig. 6a). In more details, the accuracy measure for moderate class can be calculated as: 4 / (1+11+4+9) = 16%, while much more promising are those of the other three classes: 90.48%, 88.89%, 78.57% for severe, lightly, and non-squeezing cases, respectively. The insufficiency in classifying "moderate" case may be related to the class imbalance situation in the training dataset. From Fig.2 we can learn that the percentage of moderate squeezing cases in the dataset are comparatively lower than other classes in Singh scheme: moderate cases have a share of 16% while other three classes approximately equal to 27%.

Moreover, if we step back and look at the confusion matrix from a binary perspective (see Fig. 6b), the Binary tree model reaches a 93.5% accuracy in classifying merely squeezing and non-squeezing cases, with only 12 out of 154 being misclassified. Although it is not possible to directly compare the binary accuracy with other training methods in literature, since different database, predictors and even cross-validation approaches are involved in each study, our results are still highly significant because our database has the most comprehensive information in terms of the quantity of training samples and predictors and our results have been validated through a standard 10-fold cross validation procedure, based on the comparison shown in Table 4.

[Table 4 approximately here]

[Figure 7 approximately here]

[Figure 8 approximately here]

Fig. 7 and Fig. 8 display the pruned tree structure of the Singh tree model and the Binary tree model, respectively. In the Decision Tree method, the tree structure *per se* represents the predictive model, with its branches reflecting the conjunctions of predictors that finally lead to the classification results.

Three thresholds concerning *SSR* can be identified from the Singh tree (Fig. 7): namely 0.235 in Node 1, 0.441 in Node 5 which separates out non-squeezing cases, and 0.207 in Node 2 which separates between severe-squeezing cases and moderate-squeezing cases. Specifically, Table 5 shows the comparison regarding the criterion of dividing squeezing degree via *SSR*. Note that unlike those empirical thresholds of *SSR* of previous models to classify squeezing degrees, the ones identified in the Singh tree are derived by the C5.0 algorithm strictly based on the information gain in entropy theory. Upon comparison, the thresholds in Singh tree are largely resemble those of Hoek, which established the applicability of the Singh tree model as Hoek's thresholds are widely used as a basis for the design of support systems (Hoek 2001). Besides, the Singh tree model takes information from other predictors into account (i.e. predictor *D*), compared to other univariate empirical

equations that only involved *SSR*, thereby leading to a more informed classification.

[Table 5 approximately here]

Fig. 9 accordingly reports the contribution of predictors used to classify squeezing intensity. Results show that *SSR* has the largest influence, in both Singh multi-class tree and the Binary tree, suggesting that it is the most important variable in squeezing classification. This justifies the common usage of *SSR* in so many previous squeezing predictive models (see Table 1). *D* and *K* are tied as the second most important predictors, with almost equivalent importance measure in both the Singh tree and Binary tree. In addition, it can be seen from Fig.7 and Fig.8 that the predictor *K* proves to be more effective in classifying binary situations than multi-class cases. Moreover, *GC* showed little importance (3.81%) while *H* has been eliminated in the Binary tree model; similarly, both *H* and *GC* have been eliminated in multi-class situations. These eliminations occurred because of three reasons: (i) The Decision Tree method tries to achieve pure classification in leaf nodes via least number of predictors and nodes. Therefore, predictors with less classifying power would be placed at the end of the tree structure, which are very likely to be pruned as an effort to keep the tree structure from being too complicated. (ii) As *SSR* is defined as the ratio of rock mass strength to vertical stress at tunnel depth, the information provided by *H* is to some extent presented by *SSR*, thereby weakening its importance. (iii) Due to the nature of this method, categorical variables such as *GC*, are particularly prone to be eliminated than quantitative variables (Hastie et al. 2009).

[Figure 9 approximately here]

3 Markovian geologic model

3.1 Markov process and the iterative Bayesian updating methodology

To account for the spatial variability of the geologic conditions in tunnels, a Markov process is used to simulate the random process in which the probability distribution of the representative geologic parameters are changing over locations (Ioannou 1987; Guan et al. 2012). Each parameter, following the continuous-space discrete-state Markov process, is characterized as a random variable whose state distribution is a function of location t_i (i.e., the distance from the tunnel portal). Based on this probabilistic framework, an iterative Bayesian updating approach is then nested in to update the distribution of such geologic parameters, using location-specific observations provided by exploration equipment, during the tunneling process.

The continuous-space discrete-state Markov process for a single geological parameter $X(t)$ with n states is completely defined by the transition intensity matrix **A**:

$$\mathbf{A} = [a_{ij}], \quad a_{ij} = \begin{cases} -c_i & i = j \\ c_i p_{ij} & i \neq j \end{cases} \tag{4}$$

where, transition probabilities p_{ij} expresses the probability that the next state of X will be j given its present state is i, and the transition intensity coefficients c_i represents the inverse of H_i, the average extent of each state. When the geologic profile of the tunnel is available, p_{ij} can be estimated through the ratio: the number of transitions from state i to j (N_{ij}) divided by the total number of transitions out of state i (N_{ix}), i.e. $p_{ij} = N_{ij} / N_{ix}$; and c_i can be estimated by computing the inverse of the average extent of each state H_i, as it follows an exponential distribution with rate parameter c_i, i.e. $H_i \sim \text{Exp}(c_i)$. Note that the Markov process is assumed to be homogeneous within sections with the same geologic history and thus the parameters p_{ij} and c_i are considered constants that are independent of the location within the section. This means it must be assessed separately for each section if the tunnel case involves several heterogeneous sections (Ioannou 1987). Each section is constrained in a range where both ends are excavated locations with revealed geologic information (i.e. An excavated tunnel face or known boring hole location) (Guan et al. 2012).

The probabilistic behavior of a Markov process over intervals is defined by the matrix of interval transition probabilities **V** (Ioannou 1987; Guan et al. 2012):

$$\mathbf{V} = [v_{ij}], \quad v_{ij} = v_{ij}(t_1 - t_0) = P[X(t_1) = j \mid X(t_0) = i] \tag{5}$$

where v_{ij} (t_1-t_0) expresses the transition probability that the geologic parameter will be in state j at location t_1, given it occupies state i at the current location t_0 (Ioannou 1987). The interval transition probability matrix **V** of the Markov process satisfies the Kolmogorov differential equation, and thus can be linked with the transition intensity matrix **A** as following:

$$\mathbf{V}(t_1 - t_0) = e^{(t_1 - t_0)\mathbf{A}} \tag{6}$$

The vector of state probabilities, namely $\mathbf{s}(t_i)$, at any location along the tunnel section of interest (t_i) can be inferred, given the initial prior distribution $\mathbf{s}(t_0)$ at starting point of the section, which is derived by the limiting state probability (Ioannou 1987).

$$\mathbf{s}(t_i) = \mathbf{s}(t_0)\mathbf{V}(t_i - t_0) \tag{7}$$

In this way, the state probability distributions of the parameter at all points along the tunnel could be obtained, yet in a prior sense. During the tunneling process, each excavated tunnel face, which serves as an observational location t_b, reveals newly observed geological information through the characterization of certain exploration techniques (Ashley et al. 1981; Ioannou 1987). Based on which, a two-step procedure aiming to iteratively update the state probabilities at any location along the tunnel ahead the tunnel face is implemented:

Step (i), first the posterior state probabilities $\mathbf{s}'(t_b)$ at exactly the observation location t_b is calculated, followed by the posterior interval transition matrix $\mathbf{V}'$, which now starts at t_b, instead of t_0, towards the end of the section:

$$\mathbf{s}'(t_b) = [s'(t_b)], \quad s'(t_b) = \frac{L_{jk}(t_b)s(t_b)}{\sum_{j=1}^{n} L_{jk}(t_b)s(t_b)} \tag{8}$$

$$\mathbf{V}' = [v'_{ij}], \; v'_{ij} = \frac{v_{ij}L_{jk}}{\sum_{j=1}^{n} v_{ij}L_{jk}} \tag{9}$$

The basis for such calculations is a likelihood value, represented by L_{jk}, to reflect the reliability of the observation methods for the geologic parameter since any exploration method is imperfect. The likelihood matrix for a particular observation method is defined as:

$$\mathbf{L} = [L_{jk}], \quad L_{jk}(t_b) = P[Y(t_b) = k \mid X(t_b) = j] \tag{10}$$

where, $Y(t_b)$ is the observation at location t_b for the geological parameter $X(t_b)$, L_{jk} denotes the likelihood of observing result k given the true parameter state is j. The closer $\mathbf{L}$ resembles an identity matrix, the more reliable the exploration techniques is.

Step (ii): once updated, one can substitute the posterior vector of state probabilities $\mathbf{s}'(t_b)$ and posterior interval transition matrix $\mathbf{V}'$, from Eqs. (8) and (9) into (7). These newly updated inputs are used in the next iteration to obtain a profile of posterior state probabilities $\mathbf{s}'(t_i)$ of the geologic parameter at any other point forward within the tunnel section. At this time, the new region starts at t_b, and such updating process is expected to run repeatedly by considering observations serially throughout tunneling towards the end point of the section.

3.2 Selected parameter for the Markovian geologic model

The geologic parameter X_R, which reflects the strength property of the surrounding rock, indicated by its uniaxial compressive strength (σ_{ci}), is modeled herein by a Markov process, with its parametric states shown in Table 6.

[Table 6 approximately here]

The Markovian geologic model takes the geologic profile of the tunnel at investigation phase, along with the laboratory test inventories about the uniaxial compressive strength of rock samples of representative rock types, as input. It outputs a profile of the vector **s** as well as the integrated strength variable $E(X_R)$ at any location t_i along the tunnel alignment. **s** represents the state probabilities of the geologic parameter X_R, computed from the Markov process using Eq. (4) ~ (7). The variable $E(X_R)$ is a scalar evaluation that represents the weighted average value of rock strength, calculated through the scalar product of **s** and another vector **m** which represents the mean values of each parametric state range (Table 6), as shown in Eq. (11).

$$E(X_R) = \mathbf{s} \cdot \mathbf{m} \tag{11}$$

3.3 Field Characterization of the geologic parameter at excavated tunnel face

A key element within the model is the selection of exploration technique at field by which the geologic parameter X_R can be reliably characterized and quantified into parametric states (see Table 6) at the excavated tunnel face. In mathematical sense, a more reliable exploration technique, represented by a more credible likelihood matrix, could empower a more accurate posterior probability calculation, as illustrated in Eq. (8) and (9). Therefore, in terms of rock strength, portable and reliable field exploration techniques are of great interests. Point-Load Index (*PLI*) or Schmidt Hammer Rebound tests (*SHR*) are widely recommended as quick and effective field estimates of rock strength, thanks to their portability and repeatability, especially in a practical engineering context like tunneling (Yagiz 2008; Aydin 2009; Karaman and Kesimal 2014). To achieve the updating calculations in Eq. (8) and (9), the results of *PLI* or *SHR* indexes need to be transformed into states, since the Markov process is designed to deal with discrete states as opposed to specific numerical values, as suggested by the transition matrix **A** and **V** in Eq. (6).

Previously, traditional face logging has been employed to determine the parametric states in the Markov process (Ioannou 1987; Guan et al. 2012); however, in this study where rock strength needs to be quantified, *PLI* and *SHR* would be more objective and reliable (Hoek and Marinos 2000). Moreover, much progress has been made to make both *PLI* and *SHR* even more practical in soft rock settings in recent years (Hoek et al. 1998; Hoek and Marinos 2000; Yagiz 2008; Aydin 2009). Although there definitely exists inapplicable range for those two techniques (i.e. a state 3 or 4 as shown in Table 6), however, for rock samples that these two techniques have both failed, a state 3 or 4 can be confidently concluded. In such situations, traditional tools such as knife

and thumbnail can be further used to differentiate between a state 3 or state 4.

4. Dynamic prediction of tunnel squeezing intensity

After training the probabilistic classifier for tunnel squeezing intensity and establishing a Markovian geologic model with rock strength property being featured, these two major components of the framework are combined through a Bayesian updating process of the most important predictor of tunnel squeezing (*SSR*), as evidenced by Fig. 9. The subsections below further explain the steps of such updating procedures to provide additional details for clarity. Fig. 10 provides a flowchart that both outlines the structure of the framework and presents detailed implementations. It should be noted although the predictor *GC* (see Table 2) can also be updated through such procedures, we exclude it due to its poor contribution in classifying tunnel intensity. For the other three predictors (namely *D*, *H*, and *K*), newly revealed geologic information is not able to update them in nature.

In Bayes terminology, the updated prediction is referred to as "posterior" relative to the very last round. Previously, via empirical models (Table 1) and the geologic information from the investigation stage, a prediction of squeezing condition along the tunnel can be obtained, but merely in a prior sense. This kind of prediction stands as a fast yet preliminary estimate due to the relatively low accuracy of data from the investigation phase. In contrast, as featured in this study, the Bayesian updating procedures that are based on newly excavated geologic information can serve as a useful complement, which enables the prediction on squeezing intensity to be used during the construction stage, and more importantly, to be adaptively updated with changing ground conditions.

[Figure 10 approximately here]

4.1 Deriving SSR variable from the selected geologic parameter X_R

Based on the profile of state probabilities and the integrated strength variable (**s**, $E(X_R)$) along the tunnel, as calculated from the Markovian geologic model, a profile of the rock mass strength variable $\overline{\sigma}_{cm}$ throughout the tunnel can be estimated using the $E(X_R)$. This is achieved via empirical relationships between rock mass strength and the intact rock compressive strength, such as the Bieniawski approach (Bieniawski 1993), Hoek's equation (Hoek and Brown 1997; Hoek and Marinos 2000), Barton's formulation (Barton 2002), etc.; and a comparison can be found in Lin (2011). Note that the choice of empirical formulation would largely depend on rock types and applicability of those methods in different settings, etc., which is beyond the scope of this paper. Furthermore, with the $\overline{\sigma}_{cm}$ value, and provided the overburden stress (γH) estimated from the predictor *H* (see Table 2) which is known before excavation, the value of *SSR* at each location t_i along the study section of the tunnel can be derived via dividing $\overline{\sigma}_{cm}$ by the overburden stress.

4.2 Implementation of the Bayesian updating procedures on SSR variable

The main idea of the updating procedures is to use the characterized information at the current excavated tunnel face (i.e. the parametric state of X_R indicated by the gauged result of certain exploration technique, for example, Point Load test) to update the state probabilities **s** at any location t_i ahead the current tunnel face along the tunnel (i.e. to update the profile of ($\mathbf{s}$, $E(X_R)$) throughout the selected tunnel section). In this sense, each excavation round is indeed an updating round, guided by Eq. (8) and (9); and the updating procedure works in an iterative process since the tunnel face sequentially advances with new geologic information (i.e. field characterization) revealed at each excavated tunnel face.

With the profile of ($\mathbf{s}$, $E(X_R)$) being updated round by round, the profile of $\overline{\sigma}_{cm}$ along the tunnel gets iteratively updated. As a result, given the fact that the overburden stress at each location would remain unchanged prior to or after updating, the profile of the *SSR* is also dynamically updated.

4.3 Deriving posterior squeezing prediction based on continuously updated SSR variable

With the predictor *SSR* being sequentially updated, therefore, via the trained Singh tree model, the prediction of squeezing intensity can also be updated. As a result, the profile regarding the probabilistic classification of squeezing intensity along the tunnel will accordingly be updated based on the profile of the *SSR* predictor during the tunneling process.

5 An Illustrative example

In demonstrating the application of the proposed framework, an example of a 3.6 km long tunnel (Miyaluo No.3 tunnel) located in southwest China, with a maximum overburden of 319m, is presented. First, a prior probabilistic prediction of the tunnel squeezing intensity is made through the geologic profile obtained in investigation phase, by using the best trained multi-class classifier (i.e., Singh-tree model). Afterward, based on the observed results regarding the rock strength property from the Schmidt Hammer Response (*SHR*) test during construction, a set of Bayesian updating procedures, embedded in the Markovian geologic model, are employed to sequentially update the profile of *SSR* predictor. Finally, posterior predictions on squeezing intensity are iteratively made via the sequentially updated *SSR* predictor.

[Figure 11 approximately here]

Fig. 11 shows the geologic profile of Miyaluo No.3 tunnel that reflects the ground conditions of the study section in the investigation phase, based on which the transition intensity matrix is inferred in Table 7. The likelihood matrix, which reflects engineers' confidence on the credibility of the field observations, are subjectively estimated upon experiences and analogies from literature (Ioannou 1987; Guan et al. 2012). Since heterogeneous rock masses intrinsically manifest highly spatial variability, a relatively conservative likelihood matrix of the observational method (i.e. *SHR* test) is adopted herein due to the complexity of the geologic conditions and the difficulty of field tests. In nature, the likelihood matrix would differ between different ground conditions, suggesting it to be a variable with location (Ioannou 1987). However, for simplicity, it has been considered as a constant during the study tunnel section (see Table 7).

[Table 7 approximately here]

During construction, the Schmidt Hammer rebound test (*SHR*) is continuously used to characterize the strength of surrounding rocks. Each tunnel face indeed serves as an observational location, with an advancing rate roughly at 1.8m per day. A consecutive 7-day observation is compiled in Table 8. When estimating the strength property of heterogeneous rock masses with mixed layers of different lithology types, a weighted average of all the observed rock properties was estimated to account for the contribution of each rock type (Hoek and Marinos 2000; Budetta and Nappi 2011). At each excavated tunnel face, Schmidt Hammer test is conducted on samples of each rock type respectively and then compute a weighted rebound index (see Table 8). Yagiz (2008) empirical relationship is used for estimating the uniaxial compressive strength (σ_{ci}) from the weighted rebound index, as given by Eq. (12)

$$\sigma_{ci} = 0.0028H_r^{2.584}, R^2 = 0.92 \quad (12)$$

where H_r represents the Schmidt Hammer respond index. The Panthi (2007) approach is employed to

estimate the profile of the rock-mass strength variable $\overline{\sigma}_{cm}$ based on the rock strength variable $E(X_R)$, as shown in Eq. 13. It should be noted this analysis uses Panthi formula as an illustration and many other sophisticated alternatives can also be chosen.

$$\sigma_{cm} = \frac{\sigma_{ci}^{1.5}}{60} \tag{13}$$

[Table 8 approximately here]

In the Bayesian updating process, two kinds of plots from two distinct perspectives can be drawn to illustrate the process. First, for any given observational location, for instance the starting point ZK163+105, Fig. 12 shows the ability of the Markovian geologic prediction approach, based on the *SHR* index observed at the current excavated tunnel face, to predict a profile of (**s**, $E(X_R)$) at any location ahead along the tunnel. For simplicity, seven specific locations ranging from ZK163+106.8 to ZK163+116.5, are selected to be representative target locations for illustration. Those target locations are also observational locations when excavated, thereby allowing the predicted results to be compared with the revealed conditions (see Table 9). On the other hand, for any target location of interest, say ZK163+116.5, multiple rounds of predictions can be summarized to evaluate the change of predictions as the tunnel face sequentially advances during construction, as shown in Fig. 13.

[Figure 12 approximately here]

[Figure 13 approximately here]

In more details, Table 9 lists all rounds of predicted $E(X_R)$ throughout the updating process. Each row, except for the last, represents the predicted integrated rock strength value at those target locations, based on the field characterization at a certain tunnel face (observation location), which corresponds to Fig. 12. On the other hand, each column shows the change of predicted strength values at certain target locations as the tunnel face advanced towards it, which corresponds to Fig. 13, as denoted by the purple solid line. For comparison, the last row of Table 9 lists the rock strength estimated from the gauged *SHR* index at each observational location as a reference. As an example, in Fig. 13 the gauged result at location ZK163+116.5 is highlighted by the red dotted line for comparison. Fig. 14 accordingly plots the error between gauged results and the predicted results at each round.

[Table 9 approximately here]

[Figure 14 approximately here]

In general, the predicted results agree well with the observed results. The errors tend to decline as the tunnel face approaches the target location, suggesting the predicted result are updated in a direction closer to the gauged results. The steadiness of the geologic conditions from ZK163+106.8 to ZK163+116.5, as indicated by a consecutive series of state 2 from *SHR* observations (see Table 8), contributes to make the predictions more

reliable during the updating process. The marked errors in Fig. 14, which reflect the difference between field observation and the very latest round of prediction, are generally less than 5MPa, which is reasonably accepted in engineering practice for estimating rock mass strength, especially in a heterogeneous background.

Ultimately, once the *SSR* are sequentially updated, the probabilistic prediction of the squeezing intensity at each point along the tunnel can thereby being updated round by round. Fig. 15 shows the predictions of squeezing intensity at all target locations in an iterative manner. Specifically, a prior prediction based merely on investigation information before excavation is included for comparison. For each observation location, a profile of prediction on squeezing intensity ahead the current tunnel face is displayed. For each target location, multiple rounds of predictions as tunnel face advances towards it are displayed.

As a result, in the construction phase where Bayesian updating procedures are featured, slight-squeezing situation is predicted at tunnel face ZK163+105 in the first round, however, predictions in later rounds have consistently suggested no squeezing problems for the range between ZK163+106.8 to ZK163+116.5. This change is intuitively related to the change of the predicted $E(X_R)$ between rounds (Table 9). A significant increase in predicted $E(X_R)$ value is seen in all target locations at Round 2 and then the values of all locations remain largely consistent from Round 2 to 6, which explains the change of prediction from slight-squeezing to non-squeezing at first and remain for the rest. Moreover, such changes of $E(X_R)$ are indeed related to the changes of field observations between each round. A parametric state 3 is observed at ZK163+105 in Round 1, whereas a series of state 2 observed afterward (see Table 8), which suggests a change of geologic condition from ZK163+105 (Round 1) to ZK163+106.8 (Round 2) as well as a range of similar geologic condition from ZK163+106.8 to 114.6.

The field monitoring station in the tunnel was established every 10 meters, and the tunnel convergence of two stations within the study range are documented as: 62.52 mm at ZK163+110 (ε=0.63%) and 52.46mm at ZK163+120 (ε=0.52%). Therefore, the predictions about the squeezing intensity agree well with the real conditions.

[Figure 15 approximately here]

6. Conclusions

In this paper we propose a new framework for dynamic and multi-class probabilistic prediction of tunnel squeezing intensity. To that end, we employ an extensively detailed database of tunnel squeezing inventories to train a predictive model that probabilistically classifies the tunnel squeezing intensity; and we establish a Markovian geologic model that stochastically models the geologic conditions. In particular, a series of Bayesian updating procedures, based on the revealed geologic information, are used to link these two components. By sequentially updating the state probabilities of the Markovian geologic parameter X_R and the dominant squeezing predictor --- strength-stress ratio (SSR), the multi-class prediction is adaptively updated with changes in ground conditions.

Given the variance of classification schemes on squeezing intensity, three multi-class tree models plus one binary tree have been trained and evaluated using cross-validation. Results suggest that the classifier based on the Singh scheme achieves the best performance with a cross-validated accuracy of 75.19%; moreover, if we take a step back to deal with binary situations (squeezing or non-squeezing) as seen in most previous research, the accuracy can reach 93.5%.

The Decision Tree method has a unique advantage, compared to other black-box supervised learning methods, such as Neural Network, that its tree structure explicitly reflects the conjunctions of predictors and the split criterion it used that finally leads to the classification results. Compared to previous univariate empirical models that only involved *SSR*, the decision tree classifier not only derives more reliable thresholds for *SSR*, as strictly calculated by C5.0 algorithm, but more importantly, it adds information from other predictors (i.e. the interaction of predictors in the tree structure) into consideration, thereby leading to a more informed classification.

From the comparison of predictor importance in both multi-class and binary situations, *SSR* is suggested to be the most important variable, Diameter (*D*) and Support stiffness (*K*) are tied in the second place, while Depth parameter *H* is probably the parameter with the least influence as it was eliminated in the pruned tree structure. *GC*, representing rock mass classes, although exhibiting little influence in binary cases, was also eliminated from the multi-class tree structure.

Moreover, a significant advantage of our framework is that: the best-trained probabilistic classifier (namely the Singh tree model), when coupled with the Markovian geologic model, can be extended to construction stage. Compared to previous predictive models that can only be employed for preliminary predictions in design stage due to the accuracy limit of the investigation information, the proposed framework can promptly reflect the change of geologic conditions and accordingly deliver a dynamic prediction on squeezing intensity. In addition,

it should be noted that, during the updating process, only the Point Load Index or Schmidt Response test is required in the field, which is portable, easy-to-use and would not interfere with the construction process. Hence, due to its computational efficiency and operational simplicity the proposed framework can serve as a pragmatic assistance to those mature methods, such as *in situ* convergence monitoring and advanced geologic forecast, to evaluate the squeezing potential under uncertainty. Although the reliable range of updating has not been perfectly determined yet, as it depends on the properties of rock mass and the stress setting, the general rule is 'the closer the better', as shown in Fig. 14. In a practical sense, one can always reserve a choice to count on the prediction results from the very latest round of updating.

As illustrated in the Miyaluo No.3 tunnel, for any target location of interests, multiple rounds of squeezing predictions have been made as the tunnel excavated towards it. Therefore, different levels of predictions, for example long-range, short-term, or immediate prediction, can be extracted as useful information towards the optimal selection of the primary-support based on the potential squeezing risk, and even the decision-making of many construction-related operations such as scheduling, resource allocation, financial planning.

Acknowledgement

This research was supported by the National Natural Science Foundation of China (Project Nos. U19A20111 and 41772329), the Sichuan Science and Technology Program (Project No. 2019YFG0460), the China State Railway Group Corporation Limited (Project No. 2017G008-F), the Chengdu University of Technology Program for Young Teachers (Project No. 10912-2019KY20-06354), the Independent Research Project of State Key Laboratory of Geohazard Prevention and Geoenvironment Protection (SKLGP2017Z001) and the EU Horizon 2020 project URBASIS (Project No. 813137). We acknowledge the colleagues in the research group of Tunneling and Underground Engineering in State Key Laboratory of Geohazard Prevention and Geoenvironment Protection and China Railway Eryuan Engineering Group for providing first-hand documents about the tunnel squeezing cases. And we appreciate the efforts of master students Yu Nie and Junyan Wu in processing the data. Their support is greatly appreciated.

Conflict of Interest

The authors declare that they have no conflict of interest.

Appendix A - Database of tunnel-squeezing history cases

The complete database of case histories employed in this work is reproduced in the Appendix A.

Appendix B – National standard for engineering classification of rock masses in China - BQ system (*GB50218-94*)

A two-step procedure is used in the BQ system to determine the rock mass rating. Then a classification table, which lists 5 ordinal classes based on the numeric range of rating, is used to determine the final rock mass class, as shown in Table B1.

[Table B1 approximately here]

In the first step, a basic quality index of rock mass *BQ* is calculated merely by two representative geologic parameters (i.e. the strength and integrity) via the following equation:

$$BQ = 90 + 3R_c + 250K_v \quad \text{(B1)}$$

where R_c (in unit of MPa) represents the uniaxial compression strength of intact rock, which can be obtained by standard laboratory test, or related to the in situ point load strength index $I_{s(50)}$ by Eq. (B2):

$$R_c = 22.82I_{s(50)}^{0.75} \quad \text{(B2)}$$

K_v, defined as the intactness of rock mass, is obtained by the fraction between the p-wave velocity in rock mass V_{pm} and the p-wave velocity in intact rock V_{pr} as shown in Eq. (B3):

$$K_v = (V_{pm}/V_{pr})^2 \quad \text{(B3)}$$

Alternatively, as suggested by the BQ system, when quantitative tests are not available in field, R_c and K_v can be estimated via a qualitative scheme. In accordance with two specified empirical tables (not listed here due to length limit), engineers can empirically estimate the R_c according to the rock type and hammer rebound, and estimate the K_v empirically according to joint number in unit area, joint openness, and joint infilling (Guan et al. 2012).

In the second step, the basic quality index of rock mass *BQ* should be further refined to get the modified value [*BQ*] (Eq. B4), considering the influences of ground water, weak structural planes, and the level of tectonic stress.

$$[BQ] = BQ - 100(K_1 + K_2 + K_3) \quad \text{(B4)}$$

Where K_1, K_2, K_3 are respectively the correction factors for the effects of ground water, orientation and inclination of dominant discontinuities, and the level of tectonic stress. In accord with three specified empirical tables (not listed here due to length limit), these factors are estimated empirically according to the engineers' assessment. After modification, the rock mass class is finally determined by comparing the [*BQ*] value with the rating in Table B1.

References

Ashley DB, Veneziano D, Einstein HH, Chan MH (1981) Geological Prediction and Updating in Tunneling-A Probabilistic Approach. American Rock Mechanics Association,

Aydan Ö, Akagi T, Kawamoto T (1993) The squeezing potential of rocks around tunnels; theory and prediction. Rock Mechanics and Rock Engineering 26:137–163.

Aydan Ö, Akagi T, Kawamoto T (1996) The squeezing potential of rock around tunnels: Theory and prediction with examples taken from Japan. Rock Mechanics and Rock Engineering 29:125–143. doi: 10.1007/BF01032650

Aydin A (2009) ISRM Suggested method for determination of the Schmidt hammer rebound hardness: Revised version. International Journal of Rock Mechanics and Mining Sciences 46:627–634. doi: 10.1016/j.ijrmms.2008.01.020

Barla G (1995) Squeezing rocks in tunnels. ISRM News Journal 2:44–49.

Barton N (2002) Some new Q-value correlations to assist in site characterisation and tunnel design. Int J Rock Mech Min 39:185–216.

Basnet CB (2013) Evaluation on the Squeezing Phenomenon at the Headrace Tunnel of Chameliya Hydroelectric Project, Nepal.

Bieniawski ZT (1993) Classification of rock masses for engineering: the RMR system and future trends. In: Rock Testing and Site Characterization. Elsevier, pp 553–573

Breiman L (2001) Random forests. Machine Learning 45:5–32.

Budetta P, Nappi M (2011) Heterogeneous rock mass classification by means of the geological strength index: the San Mauro formation (Cilento, Italy). Bulletin of Engineering Geology and the Environment 70:585–593. doi: 10.1007/s10064-011-0351-1

Chern JC, Yu CW, Kao HC (1998) Tunneling in squeezing ground.

Dalgıç S (2002) Tunneling in squeezing rock, the Bolu tunnel, Anatolian Motorway, Turkey. Engineering Geology 67:73–96.

Dwivedi RD, Singh M, Viladkar MN, Goel RK (2013) Prediction of tunnel deformation in squeezing grounds. Engineering Geology 161:55–64.

Einstein HH (2007) Reducing Uncertainty Through Updating-From Experiments to the Observational Method. International Society for Rock Mechanics,

Feng X, Jimenez R (2015) Predicting tunnel squeezing with incomplete data using Bayesian networks. 195:214–224. doi: 10.1016/j.enggeo.2015.06.017

Feng X, Jimenez R (2014) Bayesian prediction of elastic modulus of intact rocks using their uniaxial compressive strength. Engineering Geology 173:32–40.

Fujun S (2010) ENGINEERING GEOLOGICAL CONDITIONS AND SPECIAL ROCKMASS STRUCTURAL CHARACTERISTICS OF JIUBAO RAILWAY TUNNEL.

Goel RK, Jethwa JL, Paithankar AG (1995) Tunnelling through the young Himalayas — A case history of the Maneri-Uttarkashi power tunnel. Engineering Geology 39:31–44. doi: 10.1016/0013-7952(94)00002-J

Goel RK, Swarup A (2006) A case history of tunnelling through difficult ground. Tunnelling and Underground Space Technology 21:362–1. doi: 10.1016/j.tust.2005.12.179

Guan Z, Deng T, Du S, et al (2012) Markovian geology prediction approach and its application in mountain tunnels. TUNNELLING AND UNDERGROUND SPACE TECHNOLOGY 31:61–67. doi: 10.1016/j.tust.2012.04.007

Hastie TJ, Tibshirani R, Friedman JH (2009) The Elements of Statistical Learning.

Hoek E, Brown ET (1997) Practical estimates of rock mass strength. International Journal of Rock Mechanics and Mining Sciences 34:1165–1186.

Hoek E, Marinos P (2000) Predicting tunnel squeezing problems in weak heterogeneous rock masses. Tunnels and tunnelling international 32:45–51.

Hoek E (2001) Big Tunnels in Bad Rock. J Geotech Geoenviron Eng 127:726–740. doi: 10.1061/(ASCE)1090-0241(2001)127:9(726)

Ioannou PG (1987) Geologic prediction model for tunneling. J Constr Eng Manage 113:569–590.

Jethwa JL (1981) Evaluation of rock pressures in tunnels through squeezing ground in Lower Himalayas.

Jimenez R, Recio D (2011) A linear classifier for probabilistic prediction of squeezing conditions in Himalayan tunnels. Engineering Geology 121:101–109.

Jing-Yu C, Huang-Zhi, Zhi-Xue L (2002) Planning, design and construction of Muzha tunnel project. Ministry of Transportation and Communication, R.O.C

Karaman K, Kesimal A (2014) A comparative study of Schmidt hammer test methods for estimating the uniaxial compressive strength of rocks. Bulletin of Engineering Geology and the Environment 74:507–520. doi: 10.1007/s10064-014-0617-5

Kimura F, Okabayashi N, Kawamoto T (1987) Tunnelling through squeezing rock in two large fault zones of the Enasan Tunnel II. Rock Mechanics and Rock Engineering 20:151–166.

Kuhn M, Johnson K (2013) Applied Predictive Modeling.

Lantz B (2013) Machine Learning with R.

Lin D-M, Shang Y-J, Sun F-J, et al (2011) Study of strength assessment of rock mass and application. Rock and Soil Mechanics 32:837–842.

Liu G, Zhang F-Y, Li X-Z, Yang Z-C (2005) Research on large deformation and its mechanism of Muzhailing tunnel. Yanshilixue Yu Gongcheng XuebaoChinese Journal of Rock Mechanics and Engineering 24:5521–5526.

Loh W-Y (2014) Fifty Years of Classification and Regression Trees. International Statistical Review 82:329–348. doi: 10.1111/insr.12016

Marinos V, Marinos P, Hoek E (2005) The geological strength index: applications and limitations. Bulletin of Engineering Geology and the Environment 64:55–65.

Panthi KK (2006) Analysis of Engineering Geological Uncertainties Related to Tunnelling in Himalayan Rock Mass Conditions.

Panthi KK, Nilsen B (2007) Uncertainty analysis of tunnel squeezing for two tunnel cases from Nepal Himalaya. International Journal of Rock Mechanics and Mining Sciences 44:67–76. doi: 10.1016/j.ijrmms.2006.04.013

Sakurai S (1997) Lessons learned from field measurements in tunnelling. TUNNELLING AND UNDERGROUND SPACE TECHNOLOGY 12:453–460. doi: 10.1016/S0886-7798(98)00004-2

Sanhui Q, Runqiu H (2005) Study on the large deformation characteristics of the soft rocks in Wushaoling tunnel. Modern Tunnelling Technology 42:7–14.

Shafiei A, Parsaei H, Dusseault MB (2012) Rock squeezing prediction by a support vector machine classifier. 46th US Rock Mechanics / Geomechanics Symposium 2012 489–503.

Shrestha GL (2006) Stress Induced Problems in Himalayan Tunnels with Special Reference to Squeezing. Fakultet for ingeniørvitenskap og teknologi

Shuishan W (2009) Key Technology to Control Serious Deformations of Soft Rock Stratum with High Ground Stress:Case Study on Baozhen Tunnel.

Singh B, Goel RK (1999) Rock mass classification: a practical approach in civil engineering. Elsevier

Singh B, Jethwa JL, Dube AK, Singh B (1992) Correlation between observed support pressure and rock mass quality. TUNNELLING AND UNDERGROUND SPACE TECHNOLOGY 7:59–74.

Singh M, Singh B, Choudhari J (2007) Critical strain and squeezing of rock mass in tunnels. Tunnelling and Underground Space Technology 22:343–350. doi: 10.1016/j.tust.2006.06.005

Sousa RL, Einstein HH (2012) Risk analysis during tunnel construction using Bayesian Networks: Porto Metro case study. Tunnelling and Underground Space Technology 27:86–100. doi: 10.1016/j.tust.2011.07.003

Steiner W (1996) Tunnelling in squeezing rocks: Case histories. Rock Mechanics and Rock Engineering 29:211–246.

Sun Y, Feng X, Yang L (2018) Predicting Tunnel Squeezing Using Multiclass Support Vector Machines. Advances in Civil Engineering 2018:1–12. doi: 10.1155/2018/4543984

SUN Y-C (2010) Research on Mechanism and Controlling Technologies of Surrounding Rock in Squeezing Ground. Institute of Geology and Geophysics, Chinese Academy of Sciences

Wu X, Kumar V, Ross Quinlan J, et al (2008) Top 10 algorithms in data mining. Knowledge and Information Systems 14:1–37.

Yagiz S (2008) Predicting uniaxial compressive strength, modulus of elasticity and index properties of rocks using the Schmidt hammer. Bulletin of Engineering Geology and the Environment 68:55–63. doi: 10.1007/s10064-008-0172-z

Ye-yan Q (2007) Research on the control technique on the large deformation of the water tunnel of the Sergu GU hydropower station. Southwest Jiaotong University

LIST OF FIGURES

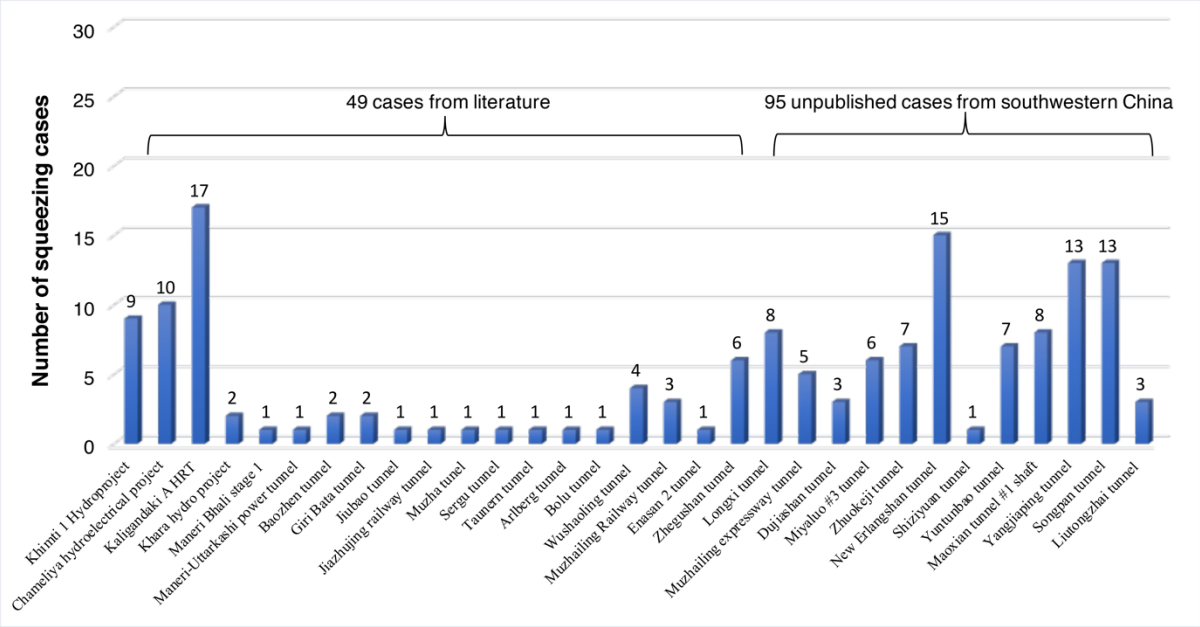

Fig. 1 The distribution of tunnel squeezing cases in the database

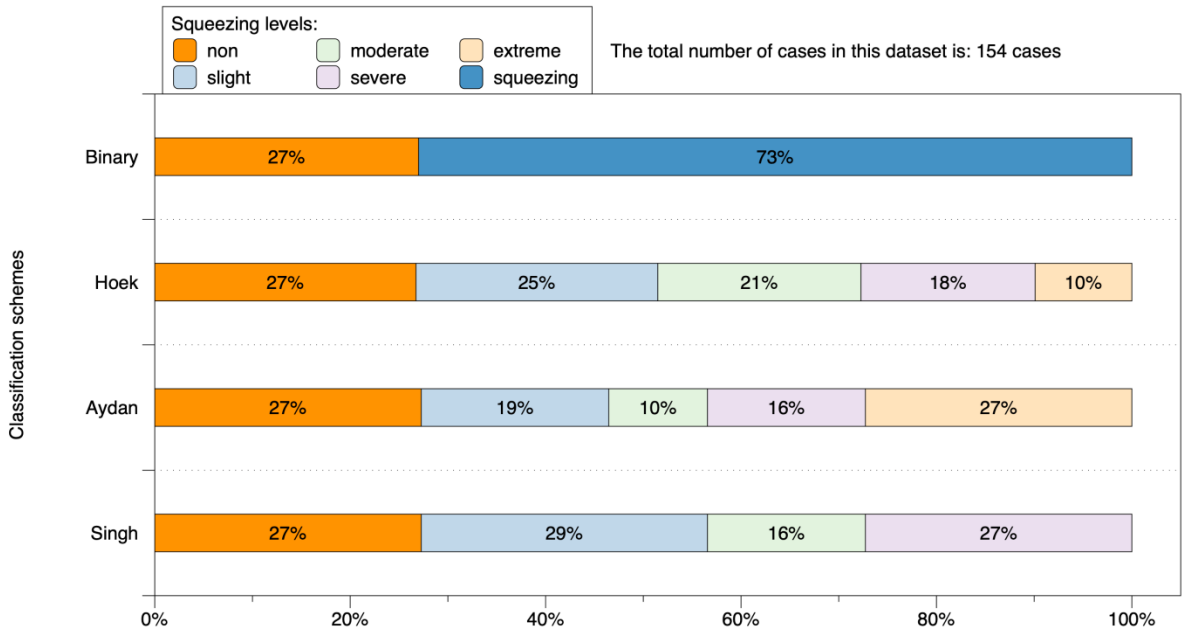

Fig. 2 The distribution of squeezing intensity of the tunnel squeezing cases in the database by different classification schemes in Table 3

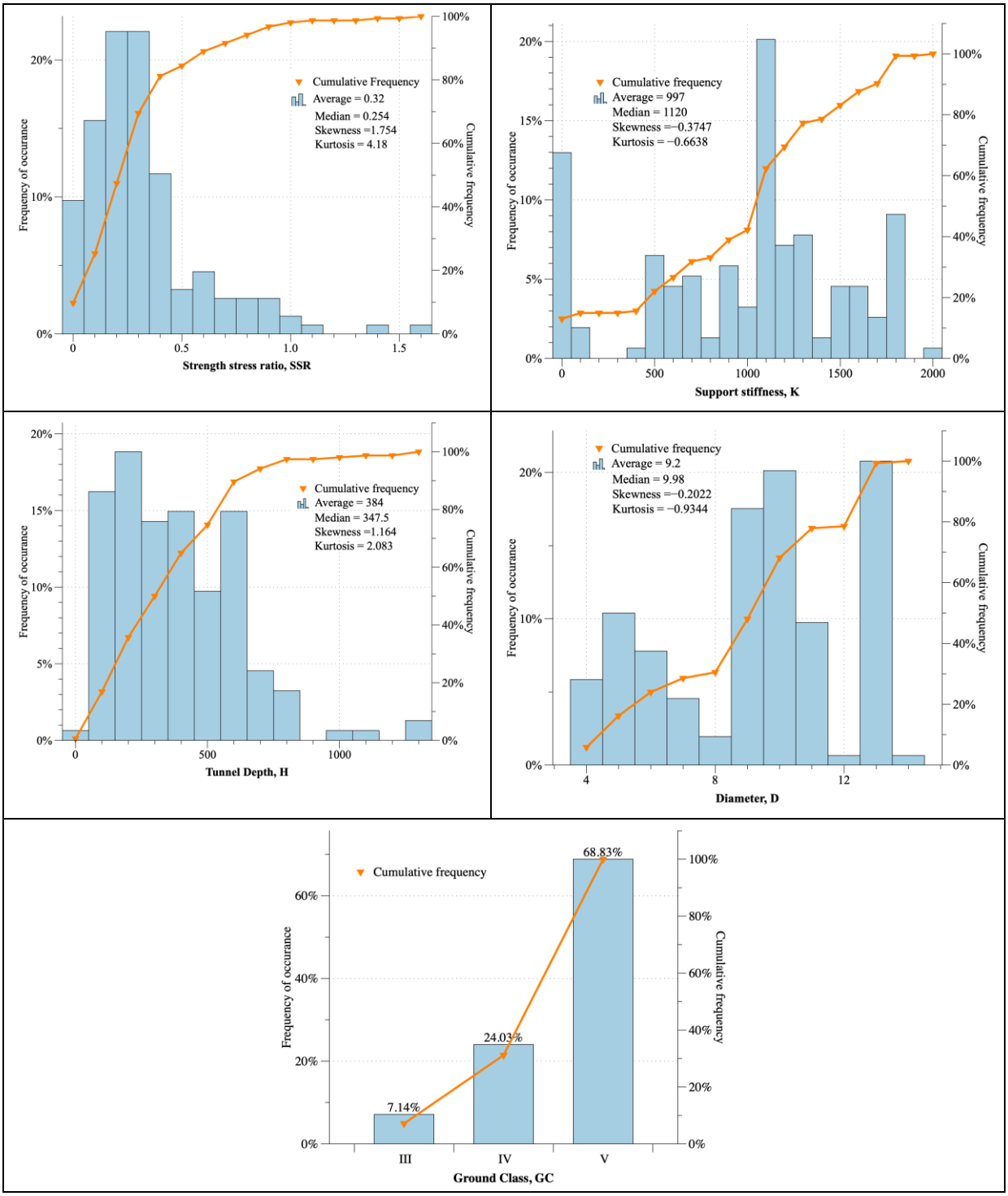

Fig. 3 Histograms and summary statistics of the five predictors considered to probabilistically classify squeezing intensity

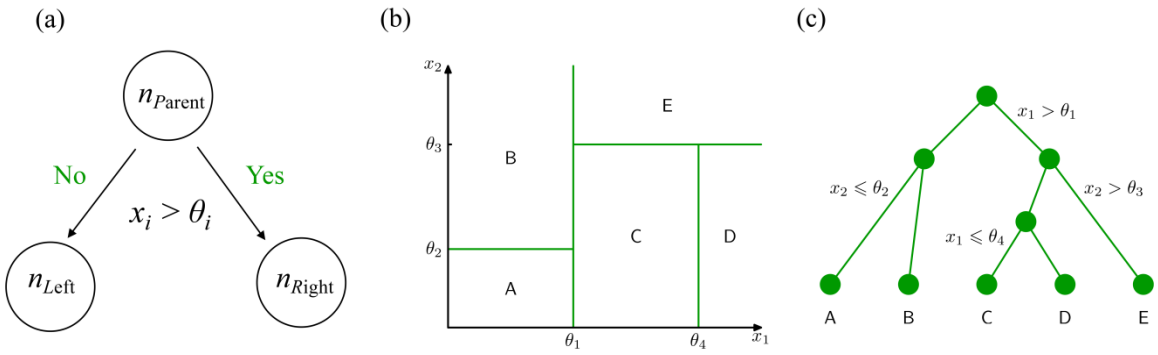

Fig. 4 Diagrams of the Decision Tree methodology

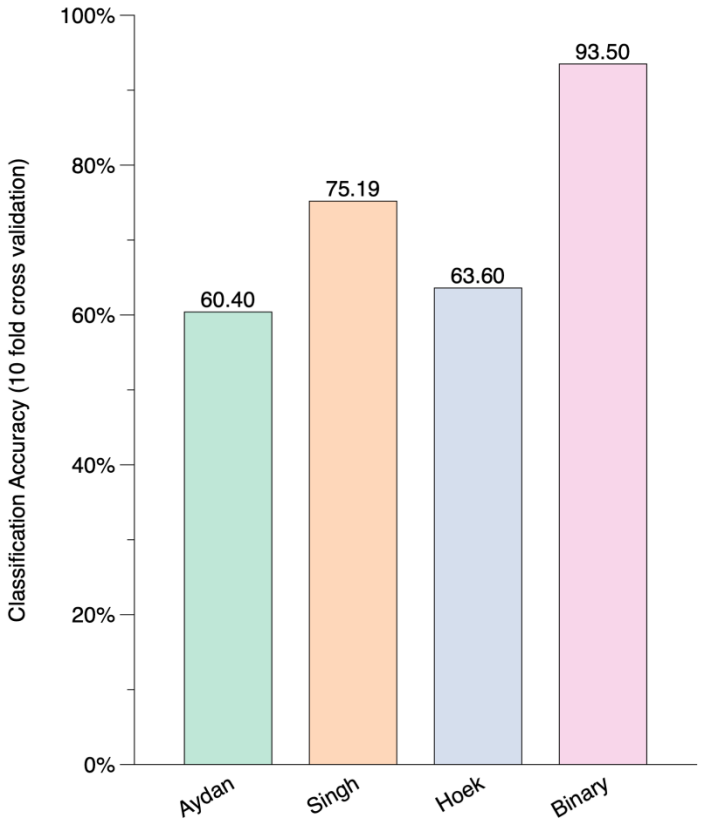

Fig. 5 Performance comparison of the trained decision trees, in a scale of 10-fold cross-validated accuracy: three multi-class trees plus one binary tree

a. Multi-class decision tree based on Singh scheme

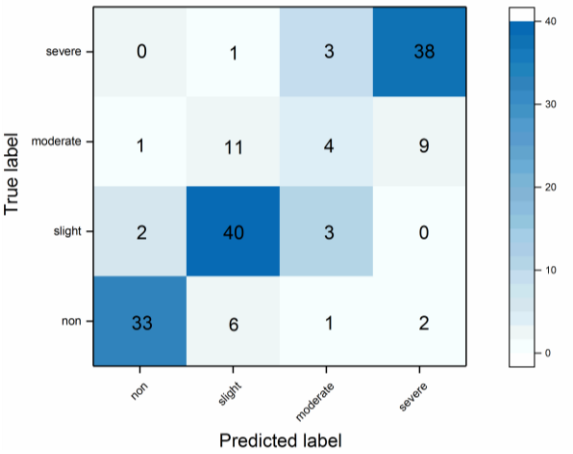

b. Binary decision tree

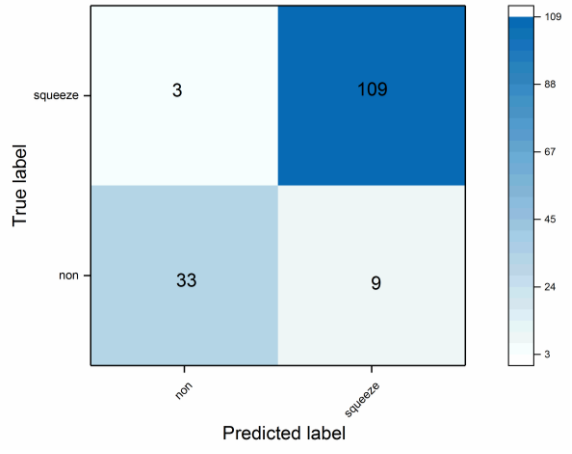

Fig. 6 Confusion matrices of the best-trained decision trees in both multi-class and binary scheme

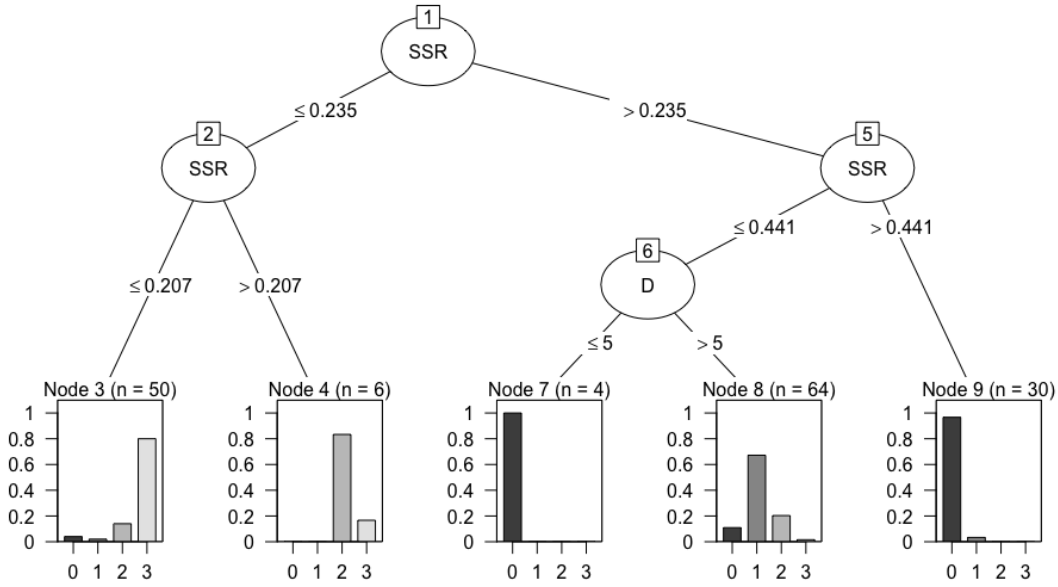

Fig. 7 Tree structure of the multi-class tree with the best performance --- Singh tree model. Each circle represents a node, with the variable by which the split is implemented shown inside, and the node number displayed at the top. In leaf nodes, the distribution of classes labelled are shown. Number *0~3* represent the class label from non-squeezing to severe squeezing; *n* means the quantity of cases in each node.

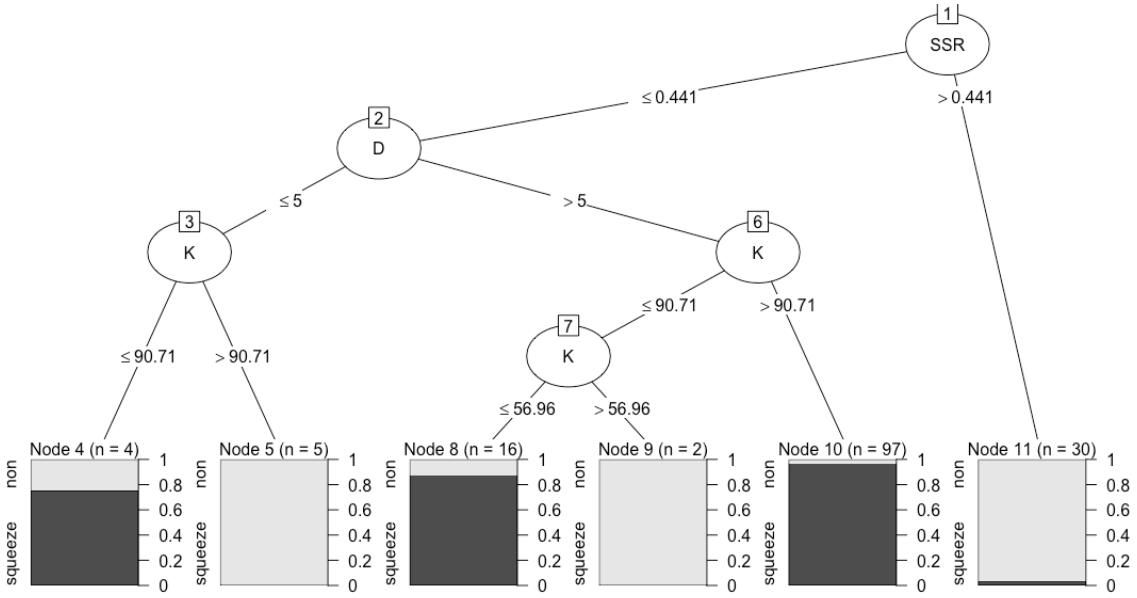

Fig. 8 Tree structure of the Binary tree model

a. Multi-class decision tree based on Singh scheme

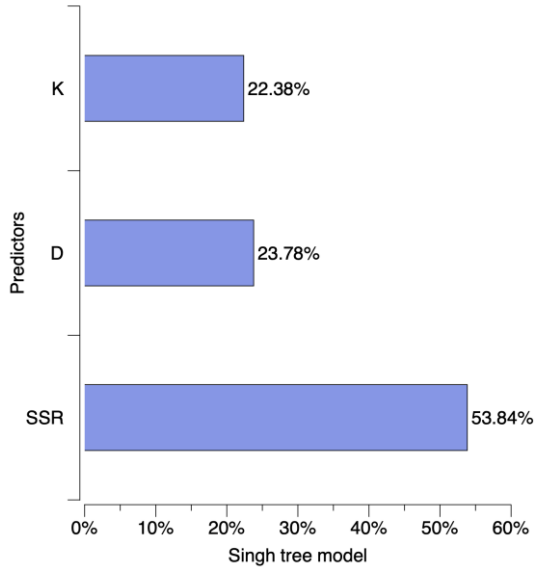

b. Binary decision tree

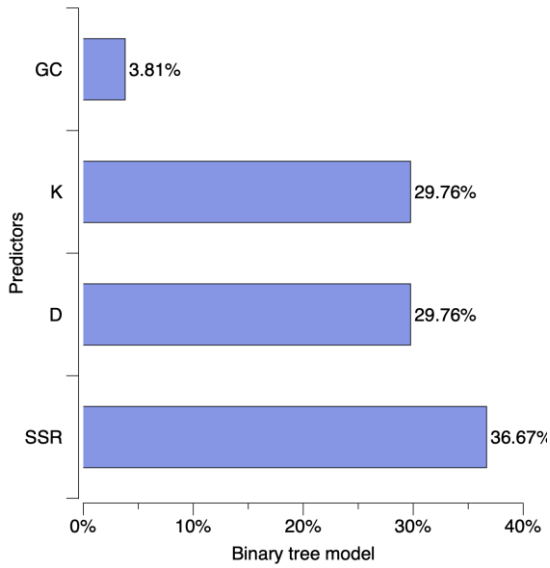

Fig. 9 Variable importance of the best-trained decision trees in both multi-class and binary scheme

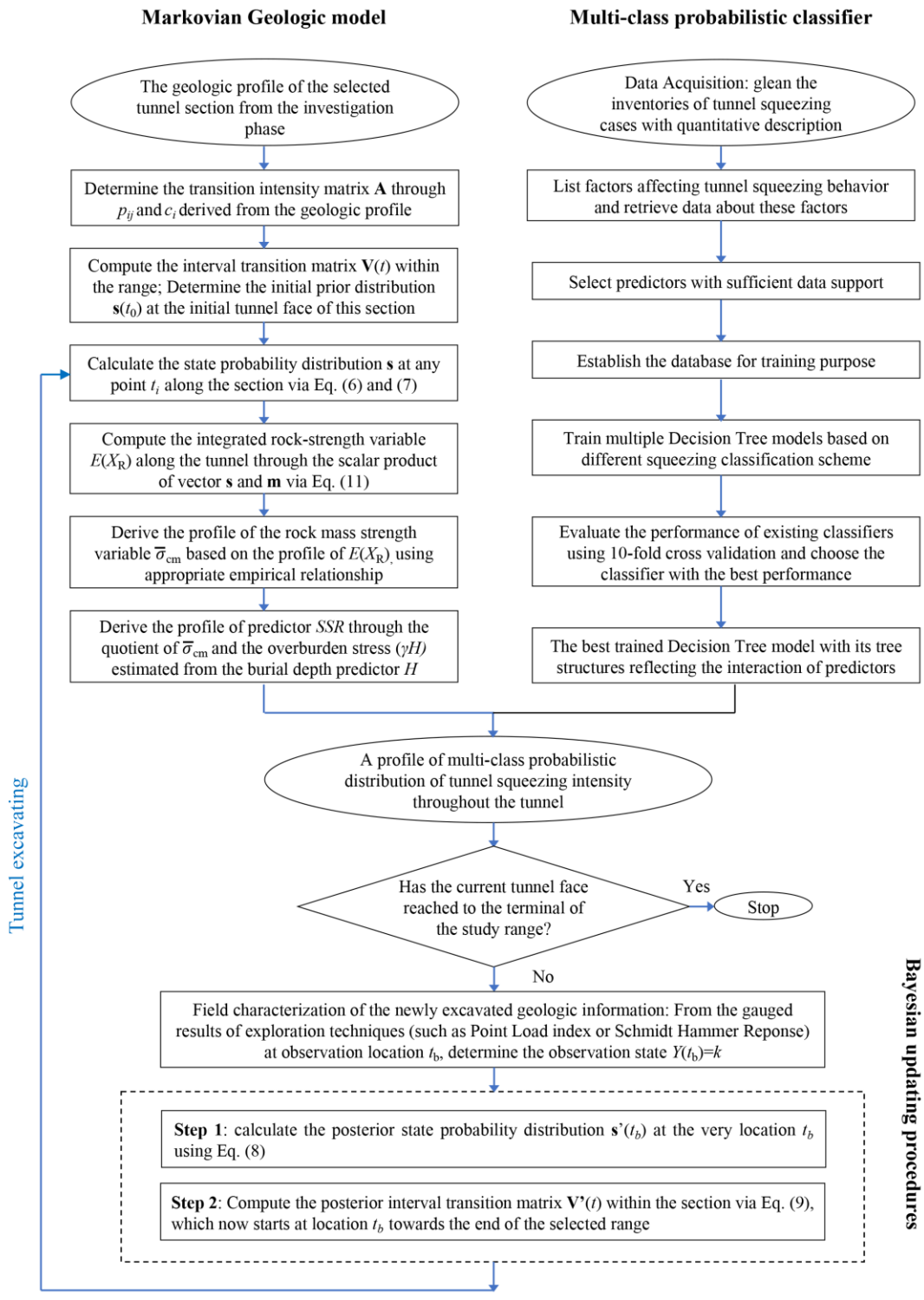

Fig. 10 Schematic diagram of the proposed framework for dynamic and probabilistic prediction of squeezing intensity

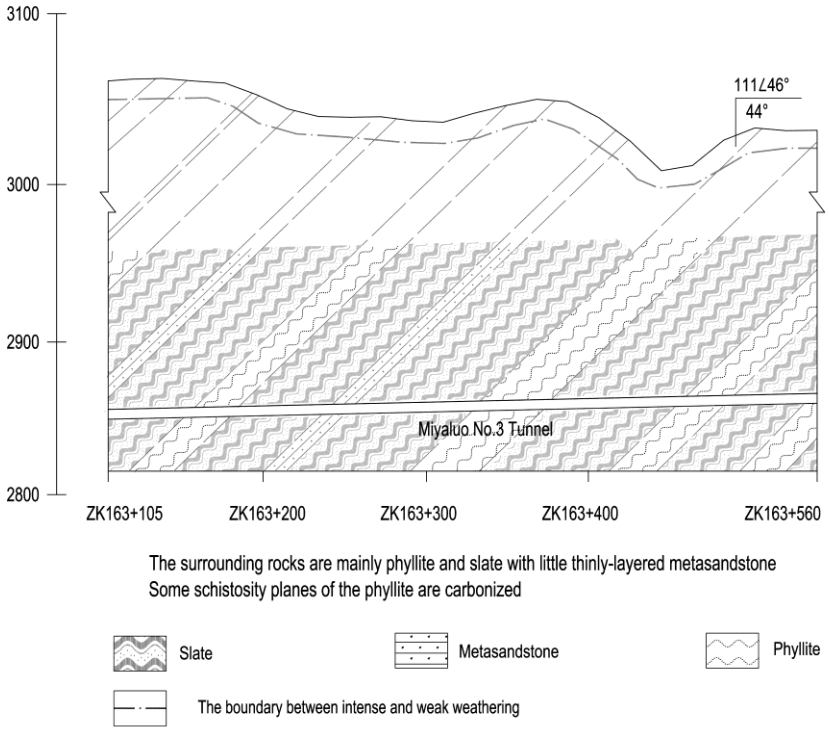

Fig. 11 The geological profile of the study section within Miyaluo No.3 tunnel in the investigation phase

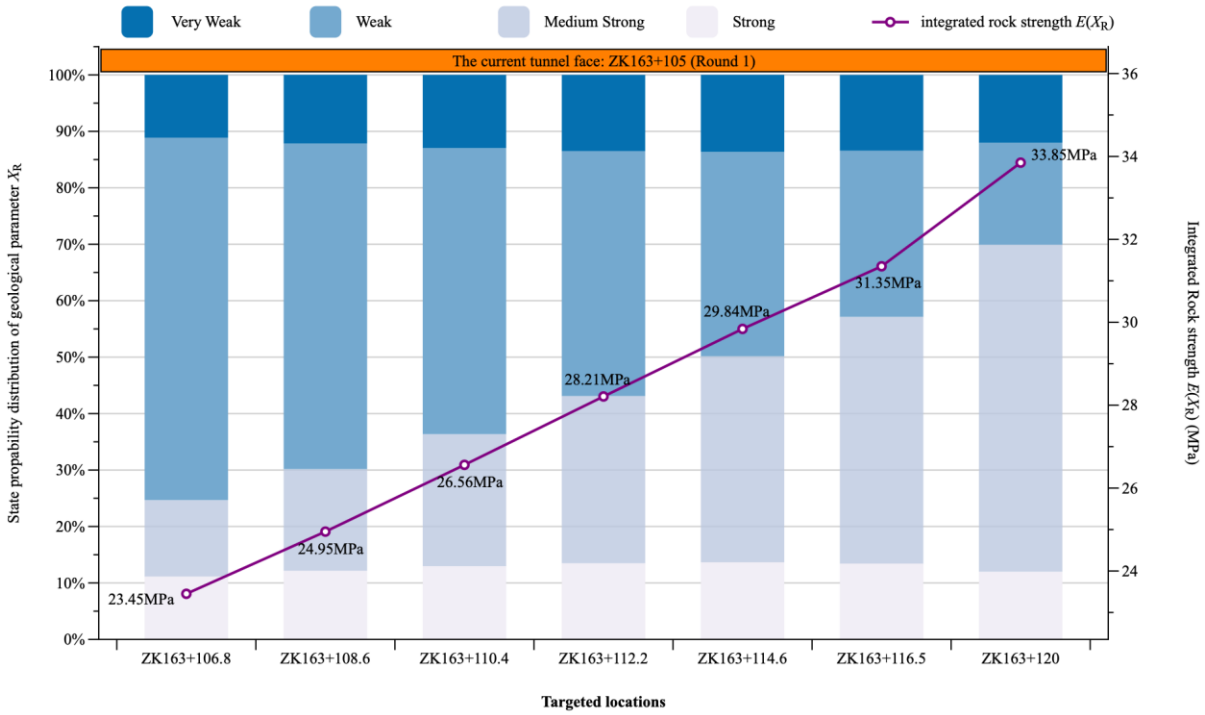

Fig. 12 Predictions on state probabilities **s** of the geologic parameter X_R and its weighted rock strength $E(X_R)$ along the study range based on the field observation at location ZK163+105

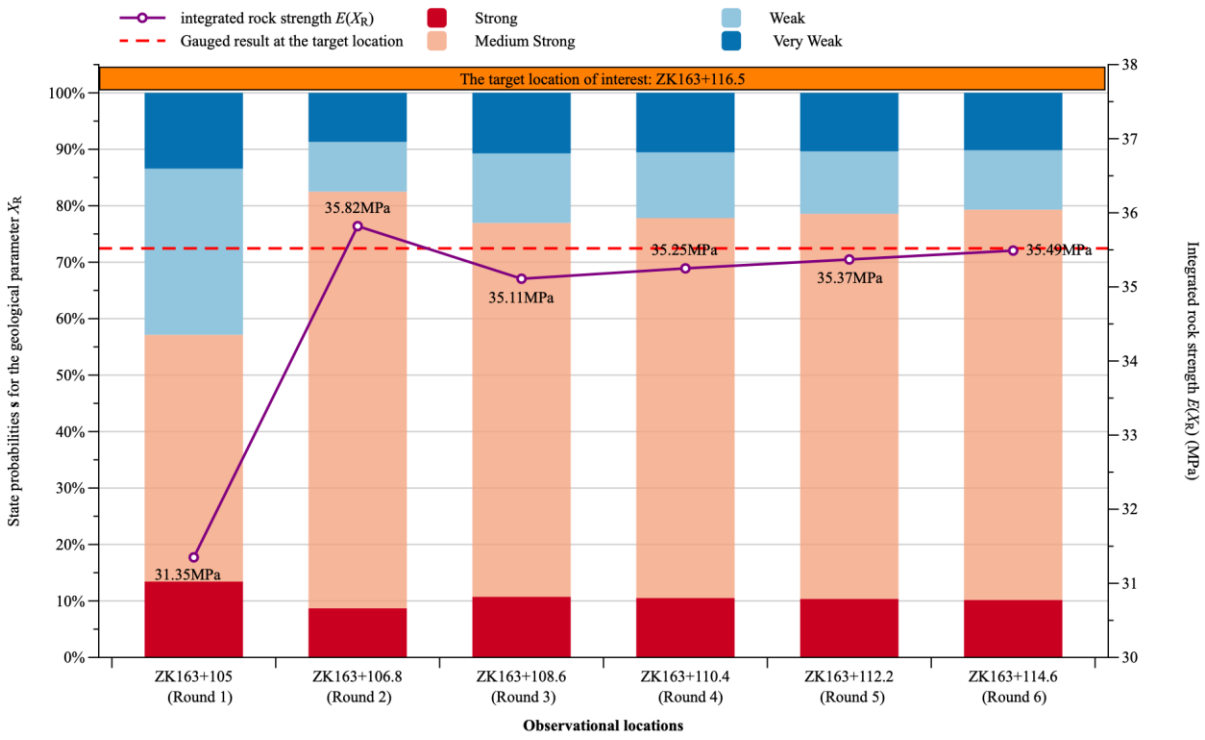

Fig. 13 The change of predictions on state probabilities **s** and the integrated rock strengths $E(X_R)$ at target location ZK163+116.5 during the updating process round by round from ZK163+105 to ZK163+114.6

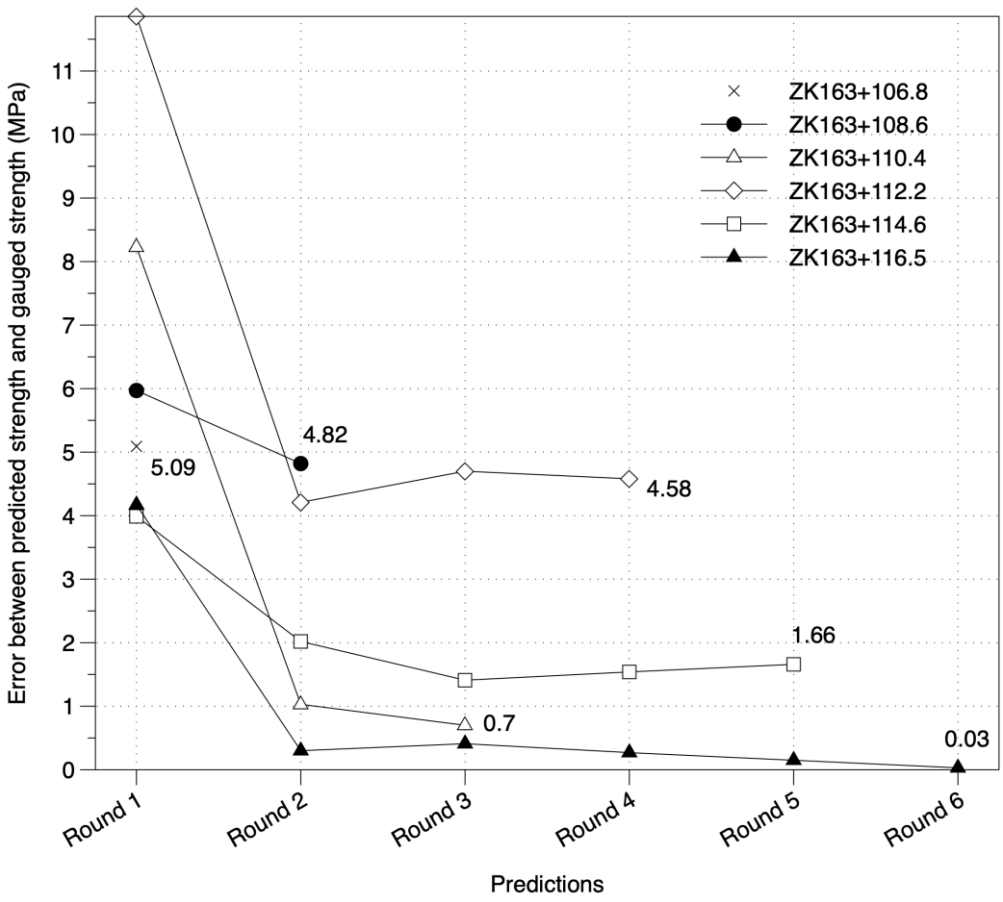

Fig. 14 The error between observed and predicted results from each round during the updating process.

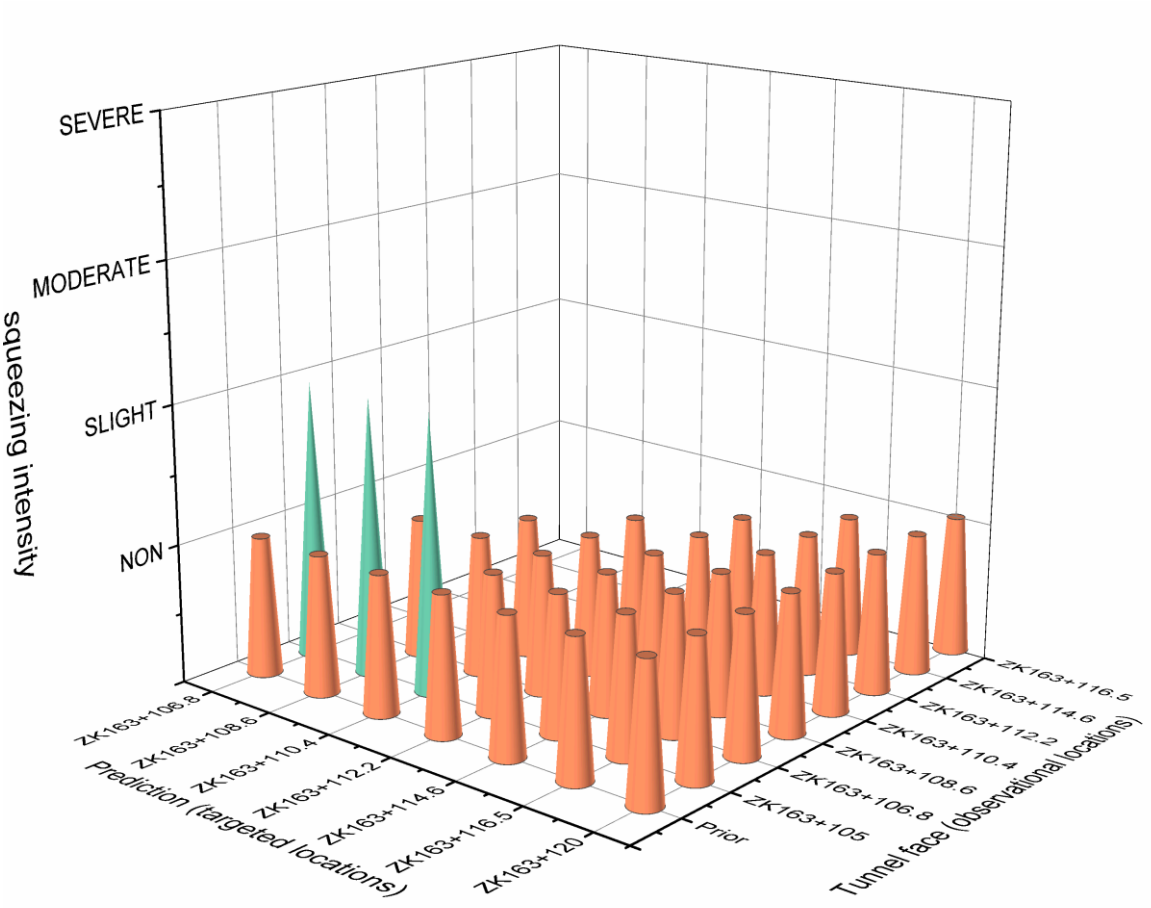

Fig. 15 Predictions on tunnel squeezing intensity of all the target locations during the updating process

LIST OF TABLES

Table 1 List of some existing empirical methods

	Formula	Source	Predictors	Dataset
Geomechanical -based methods	$H \geq 350Q^{\frac{1}{3}}$	Singh (1992)	*H*, *Q*	39 cases
	$H \geq 275N^{0.33}B^{-0.1}$	Goel (1995)	*H*, *B*, *N*	99 cases
	$\varepsilon = \frac{D^{0.12}H^{0.81}}{10.5N^{0.27}K^{0.62}}$	Dwivedi (2013)	*H*, *D*, *N*, *K*	63 cases
Competence factor-based methods	$N_c = \sigma_{cm}/\gamma H$	Jethwa (1981)	N_c, γ, *H*, σ_{cm}	-
	$\alpha = \sigma_{ci}/\gamma H$	Aydan (1996)	α, γ, *H*	Cases in Japan
	$\sigma_{cm}/\gamma H$	Barla (1995)	σ_{cm}, γ, *H*	-
	$\sigma_\theta/\sigma_{cm}$	Bhasin and Grimstad (1996)	σ_θ, σ_{cm}	-
	$\varepsilon = (0.2 - 0.25\frac{p_i}{\gamma H})[\frac{\sigma_{cm}}{\gamma H}]^{(2.4\frac{p_i}{\gamma H}-2)}$	Hoek (2000; 2001)	p_i, γ, *H*, σ_{cm}	16 cases
Probabilistic methods	Naïve Bayes classifier	Feng (2015)	*D*, *K*, *H*, *SSR*, *Q*	166 incomplete cases
	Logistic regression	Jimenez (2011)	*H*, *Q*	62 cases
	Support Vector Machine	Sun (2018)	*D*, *K*, *H*, *Q*	117 cases
	Support Vector Machine	Shafiei (2012)	*H*, *Q*	198 cases

Notation: N_c (or α) competency factor (also called "strength stress ratio (*SSR*)"), σ_{cm} rock mass uniaxial compressive strength (MPa), γ rock mass specific weight (MN/m^3), *H* depth of tunnel (m); *Q* rock tunneling quality index; *N* rock mass number (or stress-free *Q*), *SRF* stress reduction factor; *B* or *D* tunnel span or diameter (m); σ_{ci} uniaxial compressive strength of intact rock (MPa), σ_θ tangential stress (MPa), ε percentage strain (ratio of tunnel closure to tunnel diameter), p_0 in situ vertical stress at tunnel depth (MPa); p_i rock support pressure (MPa); *K* support stiffness (MPa).

Table 2 List of the predictors employed in the training process

Predictor	Description	Deriving methods
SSR	Strength-stress ratio	$\sigma_{cm}/\gamma H$
GC	Surrounding rock classes based on BQ system	$[BQ] = 63.029In(Q) + 327.5$[a]
H	Burial Depth	Measured on tunnel profile map
D	Tunnel diameter	$D = \sqrt{4A/p}$[b]
K	Support stiffness	$K = K_c + K_{sb} + K_b$[c]

Note: [a] [BQ] represents the modified quality index of rock mass in BQ system. As many squeezing cases in the database are constructed in China where BQ system is the routine procedure for evaluating rock mass quality, the Q values documented in other tunnels are converted by the empirical correlation (Yan et al. 2009);
[b] A is cross-sectional area of tunnel;
[c] K_c, K_{sb} and K_b respectively represent the stiffness of shotcrete linings, steel sets and rock bolts. For details, please refer to Feng (2015).

Table 3 Classification scheme of the squeezing intensity

Squeezing Level /%	Singh (1999)	Aydan (1993)	Hoek (2000)
No squeezing	$\varepsilon \leq 1$	$\varepsilon_\theta^a / \varepsilon_\theta^e \leq 1$	$\varepsilon_t \leq 1$
Slight	$1 < \varepsilon \leq 3$	$1 < \varepsilon_\theta^a / \varepsilon_\theta^e \leq 2.0$	$1 < \varepsilon_t \leq 2.5$
Moderate	$3 < \varepsilon \leq 5$	$2 < \varepsilon_\theta^a / \varepsilon_\theta^e \leq 3.0$	$2.5 < \varepsilon_t \leq 5.0$
Severe	$\varepsilon > 5$	$3 < \varepsilon_\theta^a / \varepsilon_\theta^e \leq 5.0$	$5.0 < \varepsilon_t \leq 10.0$
Extremely heavy	-	$\varepsilon_\theta^a / \varepsilon_\theta^e > 5.0$	$\varepsilon_t > 10.0$

Note: ε and ε_t both represent "percentage strain", which is defined as the ratio of tunnel closure to tunnel diameter; ε_θ^a is the peak tangential strain at the periphery of the tunnel and ε_θ^e is elastic strain (Singh et al. 2007).

Table 4 A comparison on binary classification accuracy between this study and other models in literature

	Sun (2018)	Feng (2015)	Shafiei (2012)	This study
Accuracy (%)	84.1	86.65	84.1	93.5
Validation approach	8-fold cross validation	10-fold cross validation	Leave-one-out	10-fold cross validation
Number of samples	117	166 (incomplete)	198	154
Training method	Support Vector Machine	Naïve Bayes	Support Vector Machine	Decision Tree
Predictors	*D, H, Q, K*	*D, K, H, SSR, Q*	*H, Q*	*D, K, H, SSR, GC*

Table 5 Classification of the tunnel-squeezing intensity based on strength stress ratio

Squeezing Level	Chern (1998)	Jethwa (1981)	Hoek (2001)	Singh-tree model
No squeezing	$0.5 \leq SSR$	$2 < SSR$	$0.45 < SSR$	$0.441 < SSR$ *or* $0.235 < SSR < 0.41$ and $D \leq 5$
Mild		$0.8 \leq SSR < 2.0$	$0.28 \leq SSR < 0.45$	$0.235 < SSR < 0.41$ and $D > 5$
Moderate	$0.25 \leq SSR < 0.5$	$0.4 \leq SSR < 0.8$	$0.2 \leq SSR < 0.28$	$0.207 < SSR < 0.235$
Severe	$SSR < 0.25$	$SSR < 0.4$	$0.14 \leq SSR < 0.2$	$SSR \leq 0.207$
Extreme heavy	-	-	$SSR < 0.14$	-

Table 6 Geologic parameter X_R of the Markov process and its state definition (reproduced from the *RMR* system (Bieniawski 1989))

Item	States			
	1	2	3	4
σ_{ci} [1]/MPa	50~100	25~50	5~25	1~5
Grading	Strong	Medium strong	Weak	Very weak
PLI[2] index	2~4	1~2	-	-
SHR[3] index	30~40	15~30	<15	-
Field estimate of rock strength used in Face-Logging routine	Requires more than one blow of a geological hammer to fracture it	Cannot be scraped or peeled with a pocket knife, specimen can be fractured with a single blow from a geological hammer	Crumbles under firm blows with point of a geological hammer, can be peeled by a pocket knife	Indented by thumbnail

Note: [1]uniaxial compress strength of intact rock; [2]Point load index; [3]Schmidt hammer response index;

Table 7 The likelihood matrix **L** and intensity transition matrix **A** for the geologic parameter X_R

A				**L**			
0.0000	0.0000	0.0000	0.0000	0.7	0.1	0.1	0.1
0.0000	-0.0203	0.0203	0.0000	0.1	0.7	0.1	0.1
0.0000	0.1099	-0.1099	0.0000	0.1	0.1	0.7	0.1
0.0000	0.0000	0.0000	-0.0000	0.1	0.1	0.1	0.7

Table 8 Quantitative results at all observation locations within the study range

Observation Location	Round	Schmidt Hammer Rebound index			σ_{ci} [b] (MPa)	Parametric state for X_R [c]
		Slate	Phyllite	wa[a]		
ZK163+105	1	45.4	12.4	19	23.43	3
ZK163+106.8	2	45.6	15.2	21.28	28.54	2
ZK163+108.6	3	45.8	16.4	22.28	30.92	2
ZK163+110.4	4	46.4	18.2	23.84	34.79	2
ZK163+112.2	5	53.95	18.83	25.85	40.07	2
ZK163+114.6	6	36.44	18.89	23.46	33.83	2
ZK163+116.5	7	51.83	17.2	24.13	35.52	2

Note: [a] Six field Schmidt Hammer tests are conducted respectively on the dominant rock types exposed at the excavated tunnel face (i.e. slate and phyllite), providing an average for each rock type. Then a weighted average rebound index is obtained based on a field observed phyllite/slate ratio.
[b] Yagiz approach used for estimating uniaxial strength of intact rock (σ_{ci}) from the weighted rebound index;
[c] the state for X_R is determined by its parametric definition in Table 6

Table 9 Predicted and observed results of rock strength at all observation locations

Observation Location	Round	Predicted rock strength $E(X_R)$ at each target location						
		ZK163+106.8	ZK163+108.6	ZK163+110.4	ZK163+112.2	ZK163+114.6	ZK163+116.5	ZK163+120
ZK163+105	1	23.45	24.95	26.56	28.21	29.84	31.35	33.85
ZK163+106.8	2		35.74	35.82	35.86	35.85	35.82	35.71
ZK163+108.6	3			35.49	35.37	35.24	35.11	34.81
ZK163+110.4	4				35.49	35.37	35.25	34.97
ZK163+112.2	5					35.49	35.37	35.11
ZK163+114.6	6						35.49	35.25
ZK163+116.5	7							35.37
Gauged results	-	28.54	30.92	34.79	40.07	33.83	35.52	-

Table B1 Engineering rock mass basic quality classification for the BQ system (LU and XU 2006)

Rock mass class	Rock mass characteristic	Rating
I	Very hard, very intact	>550
II	Very hard, intact Hard, very intact	550 - 451
III	Very hard, crushed Hard, intact Soft, very intact	450 - 351
IV	Very hard, very crushed Hard, crushed – very crushed Soft, intact – crushed Very soft, very intact - intact	350 - 251
V	Soft, very crushed Very soft, crushed – very crushed Decomposed	≤ 250

Equations in latex

Eq1:
gain(split=X)=info(t)-info{}_{X}(t)

Eq2:
info(n)=-\sum_{i=1}^{k}{p}_{i}\cdot log{}_{2}{p}_{i}

Eq3:
info{}_{X}(t)=\frac{\left| {n}_{Left} \right|}{\left| n \right|}\cdot info({n}_{Left})+\frac{\left| {n}_{Right} \right|}{\left| n \right|}\cdot info({n}_{Right})

Eq4:
{\bf{A}} = [a_{ij}],

{a_{ij}} = \left\{ {\begin{array}{*{20}{c}}
{ - {c_i}}&{i = j}\\
{{c_i}{p_{ij}}}&{i \ne j}
\end{array}} \right.

Eq5:
{\bf{V}} = [{v_{ij}}],

v_{ij} = {v_{ij}}({t_1} - {t_0}) = P[X({t_1}) = j|X({t_0}) = i]

Eq6:
{\bf{V}}({t_1} - {t_0}) = {e^{({t_1} - {t_0}){\bf{A}}}}

Eq7:
{\bf{s}}({t_i}) = {\bf{s}}({t_0}){\bf{V}}({t_i} - {t_0})

Eq8:
{\bf{s}}'({t_b}) = [s'({t_b})],

s'({t_b}) = \frac{{{L_{jk}}({t_b})s({t_b})}}{{\sum\limits_{j = 1}^n {{L_{jk}}({t_b})s({t_b})} }}

Eq9:
{\bf{V}}^{'} = [v_{ij}^{'}],

{v_{ij}}^{'} = \frac {{v_{ij}L_{jk}}}{\sum_{j=1}^{n} {v_{ij}L_{jk}}}

Eq10:
{\bf{L}} = [L_{jk}],